

Numerical Study of the Distribution of Temperatures and Relative Humidity in a Ventilated Room Located in Warm Weather

J. Serrano-Arellano¹, J. M. Belman-Flores^{2,*}, I. Hernández-Pérez³,
K. M. Aguilar-Castro³, E. V. Macías-Melo³, F. Elizalde-Blancas²,
J. M. Riesco-Ávila² and F. J. García-Rodríguez⁴

Abstract: In the present study, an analysis of the heat and mass transfer in a ventilated cavity in a warm climate zone was carried out to analyze, among others, the temperatures and percentage of relative humidity (*RH*). The governing equations of the mathematical model were solved through the finite volume method. We used the *k-ε* turbulence mode to find the results of the variables of interest in seven climate records on a given day. The velocity of the inlet flow of the air-H₂O mixture was varied through the Reynolds number (*Re*) from 500 to 10000. The outdoor weather conditions considered were solar radiation, ambient temperature, and *RH*. It was found that at low velocities, flow recirculation was formed inside the cavity which increased the temperature and concentration of *RH*. For *Re*=5000 the flow is predominantly forced, which tends to set the values of temperature and *RH* as 20°C and 20% respectively. The values of the *RH* increase in the afternoon hours when the solar radiation decreases to the value of zero. However, the mass transfer through the values of *Sh* is maintained with similar values in the seven weather records. It was concluded that when air conditioning supplies air at speeds higher than 0.26 m/s at low temperatures it produces cooling with low *RH*, this causes discomfort, illness and/or discomfort to the users.

Keywords: Heat transfer, mass transfer, solar radiation, turbulence.

Nomenclature

C=concentration of chemical specie, *Kg/m³* or *ppm*.

C_∞=concentration of reference chemical specie, *Kg/m³* or *ppm*.

C_{inlet}=concentration of chemical specie at the mixture inlet, *Kg/m³* or *ppm*.

¹ Instituto Tecnológico Superior de Huichapan, El Saucillo, Huichapan, 42411, México.

² Universidad de Guanajuato, Palo Blanco, Salamanca, 36885, México.

³ Universidad Juárez Autónoma de Tabasco, Cunduacán, Tabasco, 86690, México.

⁴ Instituto Tecnológico de Celaya, Col. Fovissste, Celaya, 38010, México.

* Corresponding Author: J. M. Belman-Flores. Email: jfbelman@ugto.mx.

Received: 25 September 2019; Accepted: 24 February 2020.

C_{outlet} = concentration of chemical specie at the mixture outlet, Kg/m^3 or ppm.
 C_{source} or C_H = concentration of chemical specie at the mixture inlet, Kg/m^3 or ppm.
 C_p = specific heat of the mixture (Air- H_2O), J/kgK .
 C_{p_m} = specific heat of the conductive wall (Air- H_2O), J/kgK .
 $C_{1\varepsilon}$, $C_{2\varepsilon}$, $C_{3\varepsilon}$, C_μ = constants of the turbulence model.
 D_{AB} = diffusion coefficient of the chemical specie from A to B, m^2/s .
 g = acceleration due to gravity, m^2/s .
 h_{ext} = convective heat transfer coefficient, $W/m^2 K$.
 H_i = aperture height at the mixture inlet (Air- H_2O), m .
 H = height of the cavity, m .
 Le = Lewis number, $Le = \alpha/D_{AB}$.
 Nu = local Nusselt number.
 \bar{Nu} = average Nusselt number.
 P = pressure of the fluid, N/m^2 .
 Pr = Prandtl number, $Pr = \nu/\alpha$.
 q = imposed heat flux at the opaque wall, W/m^2 .
 $q_{conv-ext}$ = exterior convective heat flux, W/m^2 .
 $q_{conv-int}$ = interior convective heat flux, W/m^2 .
 $q_{rad-ext}$ = exterior radiative heat flux, W/m^2 .
 Re = Reynolds number, $Re = u_{inlet} \rho H_i / \mu$.
 Sh = local Sherwood number.
 \bar{Sh} = average Sherwood number.
 T = temperature, $^{\circ}C$, K .
 $T_{average}$ = average temperature of the mixture (Air- H_2O) inside of the cavity, $^{\circ}C$, K .
 T_m = temperature of the conductive wall, $^{\circ}C$, K .
 T_{inlet} = temperature of the mixture (Air- H_2O) at the inlet, $^{\circ}C$, K .
 T_{outlet} = temperature of the mixture (Air- H_2O) at the outlet, $^{\circ}C$, K .
 u_{inlet} = horizontal component of velocity at the inlet, m/s .
 u = x component of velocity, m/s .
 v = y component of velocity, m/s .
 W = width of the cavity, m .
 W_m = thickness of the opaque wall, m .
 x = distance along x coordinate, m .
 y = distance along y coordinate, m .

Greek symbols

α = thermal diffusivity, m^2/s .
 β_T = volume expansion coefficient K^{-1} .
 ε^* = Emissivity.
 ε = rate of dissipation of k , m^2/s^3 .
 $\bar{\varepsilon}_T$ = overall effectiveness coefficient for temperature distribution.
 $\bar{\varepsilon}_C$ = overall effectiveness coefficient for concentration distribution.

k =turbulence kinetic energy, m^2/s^2 .

λ =thermal conductivity of the mixture (Air- H_2O), W/mK .

λ_m =thermal conductivity of the conductive wall, W/mK .

μ =dynamic viscosity of the mixture (Air- H_2O), $Kg/m s$.

ρ =mixture density (Air- H_2O), Kg/m^3 .

σ =Stefan-Boltzmann constant, $5.67 \times 10^{-8} W/m^2 K^4$.

1 Introduction

Currently, several studies available in the literature have analyzed the influence of weather conditions on the behavior buildings. These studies are essential because the human being who lives in urban areas spends more than 90% of their time in closed spaces [Larsen (2006)]. A study of fluid flow and mixed convection in complex geometry as a square enclosure with lower temperature sliding lid was conducted. The nanofluid medium used was a water-based nanofluid and Al_2O_3 . The effective viscosity and thermal conductivity of the solid-liquid mixture were determined. The local Nusselt number picked up at different spots on the hot wall length in correlation with the Richardson number were found. And the average Nusselt number showed linearity with respect to the variation of the nanoparticles volume fraction [Arefmanesh, Najafi and Nikfar (2010)]. Nicolás et al. [Nicolás and Bermúdez (2011)] conducted a study of mixed convection viscous incompressible fluid flows in rectangular cavities. The unsteady Boussinesq approximation for the study was considered. The results were obtained with a numerical method. The aspect ratios, Grashof numbers and Reynolds numbers were reported. The Fluid motion was not stronger and has some monotonic growth as A (A=ratio of the height to the width) are increases or decreases were found.

Therefore, it is desirable to have thermal comfort conditions in the spaces used by inhabitants. However, in thermal studies of rooms, it is necessary to propose a mathematical model that can predict the behavior of the study variables. For this purpose, researches use the tool known as Fluid Dynamics Computations (CFD) [Blazek (2001); Xamán and Gijón-Rivera (2015)]. CFD predict the values of the variables; however, all part of the physics of fluid behavior. Predicting the movement of a fluid is a complex task, several models have been proposed to solve the Navier-Stokes equations [Łukaszewicz and Kalita (2016)], with which the fluid movement can be predicted, however, to apply them to particular cases several considerations must be taken. In addition to the complexity of the differential equations that predict the movement of the fluid other equations are coupled to them; for example, the energy equation, the chemical concentration equation, the equations of the turbulent variables, etc., mentioned here the turbulence, when the problem is solved in a turbulent flow regime. Modeling turbulence is a challenge due to the random behavior of the study variables; therefore, various study models have been developed to predict the variables of interest. Analyzing the context already discussed, there is an interest in solving the equations that predict the behavior of temperature and humidity as concentrations of water vapor in an indoor space. Therefore,

a literature review of the solved problems related to this subject was performed. Studies of cavities were found in two classifications of closed cavities, which mainly study the behavior of the flow by natural convection. For instance, Das et al. [Das and Basak (2016)] conducted a study of solar gain through different materials. This study is focused on the analysis of discrete heat sources in which the heat transfer by natural convection is involved. In the study, the geometry of the cavity was either rectangular or triangular along with discrete heat sources. The numerical solution was obtained with the finite element technique. The local and average Nu values were shown along with the flow patterns, the maximum efficiency of the heat transfer for the configurations and the flow patterns for different values of Ra . Dou et al. [Dou and Jiang (2016)] developed a numerical study of the flow instability and heat transfer by natural convection in a differentially heated cavity with thin wire on the left vertical wall. The numerical model was solved with the finite volume technique, the parameters varied were; the position of the thin wire, the number of thin wires, the Ra number. It was found that the maximum efficiency of heat transfer was when the thin wire was located in the center of the vertical wall, it was also found the increase of Nu with the increase of Ra . Mehedi et al. [Mehedi, Tahzeeb and Islam (2017)] conducted a numerical study of the heat transfer by natural convection in a closed cavity with air flow with industrial and residential applications. The numerical simulation was carried out through the ANSYS FLUENT 12.0 program in a laminar flow regime, in a permanent and transitory state. The results of the heat transfer were compared through Nu values. Kouroudis et al. [Kouroudis, Saliakellis and Yiantsios (2017)] developed a numerical study of a closed cavity with natural convection flow. A constant heat flow condition was applied to the right vertical wall. The numerical solution was obtained with the finite element technique. The parameters of the study were the number of Ra . The results showed the components of temperature, velocity, and flow patterns with Ra increments. Kefayati [Kefayati (2017)] conducted a numerical study with the finite difference method of Lattice Boltzmann for a non-Newtonian fluid considered as a nanofluid with entropy generation through fluid friction. In the study, this author analyzed heat and mass transfer. The parameters varied were; Ra number, Da number, Pr number, buoyancy ratio number N_b , power-law index n , Lewis number Le , Thermophoresis parameter N_t , and Brownian motion parameter N_b , as can be seen, considered a large number of parameters to analyze. The results showed that the increase in power-law index alters heat and mass transfer, the increase in the Lewis number augments mass transfer while it causes heat transfer to drop. Miroshnichenko et al. [Miroshnichenko and Sheremet (2018)] developed a numerical study of the conjugated heat transfer by natural convection in a closed cavity in a turbulent flow regime. Inside the cavity, the authors placed a solid wall with a radiative surface with a variation of the emissivity and conductivity values. In the results, they found an increase close to 42% of the convective heat with an increase in the number of Nu . Parmananda et al. [Parmananda, Dalal and Natarajan (2018)] presented a numerical study of a three-dimensional differentially heated cavity with the effect of thermal radiation. Four different configurations were analyzed to compare the variation of the local Nu number

and the temperature distribution. The study showed the maximum heat transfer for the minimum entropy production along with the most efficient configuration in heat transfer. Kefayati [Kefayati (2019)] developed a number study with the Lattice Boltzmann method of natural convection in a porous cavity. The study parameters were Ra number, Da number, porosity ε , and number of Bn . The results showed the increase of the heat transfer and the unyielded section diminishes with the increase of the number of Ra for variation of the values of the numbers of Ra and Da and with the increment of the Bn number the heat transfer decreases. Once the heat and mass transfer by natural convection was addressed, it was observed that the studies are focused on the different parameters of each study. However, in natural convection, no studies have addressed the issue of heat and mass transfer as a concentration of water vapor.

Studies of ventilated cavities are also available in the literature, many of which have a bioclimatic approach to determine thermal comfort or air quality in rooms, offices and other spaces for a particular use. For instance, some of the parameters that are addressed in these studies are construction materials, outdoor weather conditions, effect of the inflow and outflow locations, etc. Yao et al. [Yao and Lin (2014)] studied numerically and theoretically the effect of different types of air supply terminals like; circular diffuser, square diffuser, perforated diffuser and double deflection grille. They performed different experiments changing the conditions of the study variables. They analyzed the flow patterns, the temperature distribution, and concentration of CO_2 . The results showed that the flow pattern is highly influenced by the type of diffuser, and they concluded that the circular diffuser was the most efficient. Yu et al. [Yu, Yang and Xiong (2015)] conducted a study of the thermal behavior of a hollow block in the buildings due to the high energy demand present in China. They proposed a ventilated hollow block wall to minimize heating or cooling thermal loads. The study was conducted with the Frequency-Domain Finite Difference (FDFD) coupled to a CFD model. They analyzed the influence of frequency, amplitude and angle phase on the incidence of the external surface and the influence on the inner surface with the heat flux amplitude. Zhang et al. [Zhang, Cheng, Fang et al. (2017)] conducted a numerical study to optimize temperatures and achieve thermal comfort together with energy savings in ventilated rooms. They modified the PVM model for thermal condition evaluation and found a difference of 0.14 on the scale of the thermal sensation vote. Further, they found that the optimum temperature was $28.5^\circ C$ and the energy saving was 7.8%. Pretrel [Pretrel (2017)] conducted a study of the interaction of water spray and smoke in a ventilated cavity. The author performed 17 experiments in a ventilated room with a fire source. He found that the water spray influences the pattern of the smoke; there is a homogenization of the flow and separation of the chemical and thermal stratification. He concluded that the energy transferred to the droplet flow is above 65%. Koufi et al. [Koufi, Younsi, Cherif et al. (2017)] conducted a numerical study of the air quality in a ventilated room using different ventilation strategies. The model was solved with the scStream code. They analyzed the ventilation effectiveness (ε_c) and the index of indoor air quality (I_{IAQ}). The ventilation flow rate was $50 \text{ m}^3/\text{h}$; the study was performed for air in a turbulent flow

regime. They found that the air quality improves after 23 min with the best efficiency (ϵ_c). Raczkowski et al. [Raczkowski, Suchorab, Połednik et al. (2018)] conducted a CFD study of the thermal comfort in a ventilated room by natural convection in which a valve was placed to introduce air from the outside. They found the temperature and velocity profiles and compared these variables with the experimental measurements, and they found that the numerical values are overestimated. Huang et al. [Huang, Yu and Yang (2018)] conducted a study of the factors that influence the behavior of a hollow block that serves as a thermal insulator. The study was done with the finite difference method and the Number of Transfer Units. They used a three-dimensional geometry to compare the results with experimental measurements. They found that the block significantly reduces heat transfer in the summer season because heat fluxes through the hollow wall are reduced by an average of 50%, and that the most critical factor in the study was the dimensions of the cavity. Singh et al. [Singh, Kumar, Ooka et al. (2018)] presented a statistical study of thermal comfort in a naturally ventilated classroom for the summer season in India. They analyzed the thermal comfort conditions in accordance with ASHRAE Standard 55, the average indoor climate conditions for the study were 30.4°C, 39.4% and 0.59 m/s of air temperature, relative humidity and flow velocity, respectively. They found that about 81% of the responses were favorable with respect to the thermal comfort. Kumar et al. [Kumar, Singh, Mathur et al. (2018)] presented a thermal comfort study similar to Singh et al. [Singh, Kumar, Ooka et al. (2018)]. They performed different actions to regulate the indoor conditions and found that the preference in the average vote of thermal comfort was when the room had high airflow rates. All of the surveyed people preferred to use the fan, 50% open windows and 40% the doors. The authors verified that the bioclimatic architecture of the building was not adequate. Harish [Harish (2018)] conducted a study of the effect of the aspect ratio of a heat source in a ventilated cubic cavity in a turbulent flow regime. The turbulence was modeled with the LES turbulence model, and the numerical technique used for solving the governing equations was finite differences. They varied the number of Gr. In the results, they showed the influence of the heat source with the flow pattern that was formed inside the cavity. Huan et al. [Huan, Wang, Wu et al. (2018)] developed a nodal model to predict the vertical temperature profile in a ventilated room. The proposed model was validated with nine experiments in different scenarios, by comparing the results, they found that the nodal model had an average error of 8.7% and a standard deviation of 5.8%. Al-Kayiem et al. [Al-Kayiem, Sreejaya and Chikere (2018)] conducted a numerical and experimental study of the influence of the location of the flow inlet in a solar chimney. The numerical study was done with the FLUENT program. The experiments were carried out in a built prototype. They found that the configuration with vertical cross section was the one that showed to be more efficient. Yamamoto et al. [Yamamoto, Ozaki, Lee et al. (2018)] conducted a study of coupling methods between energy simulation (ES) and CFD programs in a room heated by natural convection. The numerical model was fed by the ES model to predict the temperature field. The results they showed were the coupling of the systems to reproduce the temperature distributions in the space of use. Macias-

Melo et al. [[Macias-Melo, Aguilar-Castro, Xamán et al. \(2018\)](#)] presented an experimental study of a ventilated rectangular cavity with a heated wall, an inlet, and an outlet for airflow. They analyzed four different configurations. They compared the experimental results with those obtained in a numerical code. They found that for a power of 200 W they obtained increases in air temperature from 4.3°C to 5.0°C in the different study configurations, for the power of 400 W, the increase was only 3.3°C. The maximum differences between the experimental and numerical results were 9.9% and 11.5% for the test of 200 and 400 W, respectively.

Shi et al. [[Shi, Liu, Wang et al. \(2019\)](#)] investigated in a ventilated porous cavity in which a forced flow was imposed and inside it contained a local source of contamination. They studied the effect of natural and forced convection with the variation of the number of Re , the number of Da , and the relative magnitude between the effective solute buoyancy and the effective external force in a porous medium (f). The results showed the flow patterns through the gradients of velocity, isolines in a steady and transient state, and the dependence of the flow pattern of the number of Re and Da . Wang et al. [[Wang, Chen and Li \(2019\)](#)] performed a numerical simulation of the temperatures in a rectangular cavity with double façades with natural ventilation by the zone methodology. The authors validated the results with experimental data. They found the influence of slat angle, air cavity thickness, and DSF height on the results of temperature and airflow rate. The maximum error they found between numerical and experimental data was 8.3%.

Finally, it can be concluded that the continuous study of closed or ventilated cavities help to understand the phenomenon of heat transfer and/or mass, as can be seen there are studies with different study parameters. However, studies that study the distribution of temperatures and the percentage of relative humidity (RH) in a room with the considerations of this study were not found. So, this paper will contribute to the better understanding of the behavior of airflow with water vapor as chemical species concentration inside a ventilated room, this will give new solutions to create better hygrothermal conditions within a building with this will facilitate the stays and/or tasks of the users within the architectural spaces for habitability.

2 Physical model of the ventilated cavity with heat and mass transfer of a mixture of air-H₂O

[Fig. 1](#) shows the physical model of the ventilated cavity; the model has been simplified to a two-dimensional square geometry with inlet and outlet openings of the air-H₂O mixture. Inside the cavity, there is a certain amount of moisture in the air generated by a wet source. The opening of the flow inlet of the air-H₂O mixture is in the lower part of the right vertical wall. Regarding the exit opening of the air-H₂O mixture, it is located on the left vertical wall. The right vertical wall is solid opaque in which a flow of heat is imposed on the outside of the surface. As a result of this thermal energy, the wall increases its temperature, and when interacting with its surroundings, heat losses are produced by convection and radiation to the external environment. In the interior, due to the temperature difference, there is convective heat flow and a variation of the mixture density. Further, there is a difference in the concentration of H₂O vapor, which also

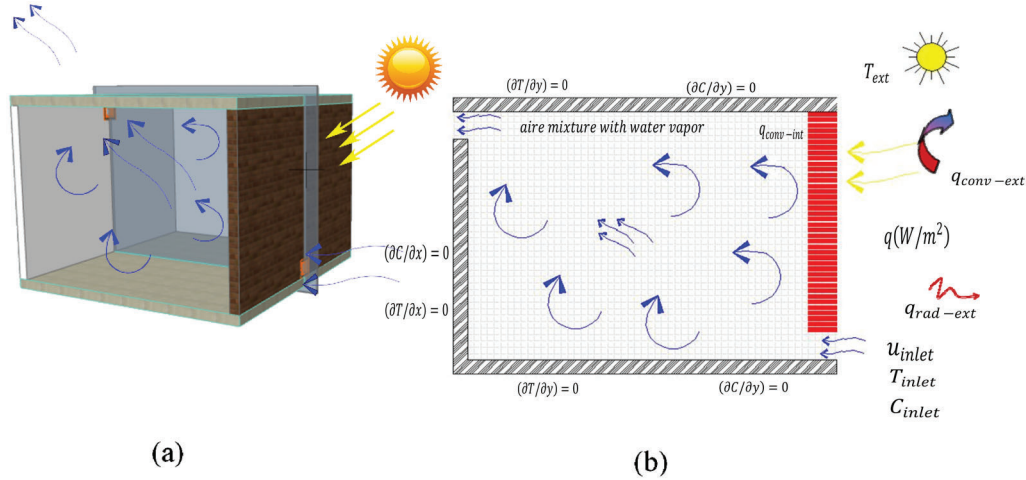


Figure 1: Physical model of the ventilated cavity

produces a density variation. When this density change occurs, the air-H₂O mixture moves. The movement thus produced is added to the forced effect by the flow supplied at the opening of the flow inlet. The flow provided in the inlet opening has a constant speed, a constant temperature, and a vapor concentration of H₂O in the air.

3 Mathematical model for the heat and mass transfer of a mixture of air-H₂O

The mathematical model consists in the representation of those governing equations that best characterize the physical behavior of the ventilated cavity. The equations presented below represent the movement of the flow through the momentum equation; the heat transfer is represented by the energy transport equation; and mass transfer is represented by the transport equation of chemical species. For the equations mentioned above, it is necessary to add the equations that model the turbulence. There are different turbulence models; in this particular case, the modeling was performed with the k - ϵ turbulence model. The system of governing equations is:

Mass conservation equation,

$$\frac{\partial(\rho u_i)}{\partial x_i} = 0 \quad (1)$$

Momentum conservation equation,

$$\frac{\partial(\rho u_i u_j)}{\partial x_j} = -\frac{\partial P}{\partial x_i} + \frac{\partial}{\partial x_j} \left[\mu \left(\frac{\partial u_i}{\partial x_j} + \mu \frac{\partial u_j}{\partial x_i} \right) - \overline{\rho u_i' u_j'} \right] + \rho g_i \beta (T - T_\infty) + \rho g_i \beta_c (C - C_\infty) \quad (2)$$

Energy conservation equation,

$$\frac{\partial(\rho u_j T)}{\partial x_j} = \frac{1}{C_p} \frac{\partial}{\partial x_j} \left(\lambda \frac{\partial T}{\partial x_j} - \rho C_p \overline{u_j T'} \right) \quad (3)$$

Transport species equation,

$$\frac{\partial(\rho u_j C)}{\partial x_j} = \frac{\partial}{\partial x_j} \left(\rho D_{AB} \frac{\partial C}{\partial x_j} - \rho \overline{u_j C'} \right) \quad (4)$$

In equations from (2) to (4) there are terms that are approximate, these are the Reynolds stresses, and turbulent heat and mass flux vector. The approximations are shown in the following equations:

$$\overline{\rho u_i u_j} = -\mu_t \left[\frac{u_i}{\partial x_j} + \frac{\partial u_j}{\partial x_i} \right] + \frac{2}{3} \rho \kappa \delta_{ij} \quad (5)$$

$$\rho C_p \overline{u_i T'} = -\frac{\mu_t}{\sigma_t} \frac{\partial T}{\partial x_i} \quad (6)$$

$$\rho \overline{u_i C'} = -\frac{\mu_t}{S_{c_t}} \frac{\partial C}{\partial x_i} \quad (7)$$

In Eq. (6), σ_t represents turbulent Prandtl number and in Eq. (7), S_{c_t} , represents turbulent Schmidt number. Moreover, the turbulent viscosity term turbulent viscosity, (μ_t) which relates the turbulent kinetic energy (k) and the turbulent kinetic energy dissipation (ε) by the Kolmogorov-Prandtl empirical expression as: $\mu_t = C_\mu \frac{\rho k^2}{\varepsilon}$. To be able to close the turbulence model the values of the turbulent kinetic energy (k) and the turbulent kinetic energy dissipation (ε) are required, this can be found in the model used by Henkes et al. [Henkes, Van Der Vlugt and Hoogendoorn (1991)]:

Turbulent kinetic energy,

$$\frac{\partial(\rho u_i \kappa)}{\partial x_i} = \frac{\partial}{\partial x_i} \left[\left(\mu + \frac{\mu_t}{\sigma_\kappa} \right) \frac{\partial \kappa}{\partial x_i} \right] + P_\kappa + G_\kappa - \rho \varepsilon \quad (8)$$

Turbulence dissipation rate,

$$\frac{\partial(\rho u_i \varepsilon)}{\partial x_i} = \frac{\partial}{\partial x_i} \left[\left(\mu + \frac{\mu_t}{\sigma_\varepsilon} \right) \frac{\partial \varepsilon}{\partial x_i} \right] + C_{\varepsilon 1} [P_\kappa + C_{\varepsilon 3} G_\kappa] \frac{\varepsilon}{\kappa} - C_{\varepsilon 2} \frac{\rho \varepsilon^2}{\kappa} \quad (9)$$

Next, the boundary conditions for the velocity components are stated, it is considered that in the solid surfaces the velocity components are zero.

The previous Eqs. (1) to (9) describe the convective movement of the mixture in a turbulent flow regime, which are expressed in the literature in developed or compact form to represent

the phenomenon under study. However, they require boundary conditions to particularize the problem to be solved. The boundary conditions in this study are shown below.

Boundary conditions for the velocity components:

	Horizontal component of velocity	Vertical component of velocity
Boundary conditions in the inlet opening of the flow of mixture air- H_2O	$u=u_{inlet}$	$v_{inlet}=0$
Boundary conditions in the outlet opening of the flow of mixture air- H_2O	$\frac{\partial u}{\partial n}=0$	$\frac{\partial v}{\partial n}=0$

where n is the normal vector to the direction of the flow

Boundary conditions in the walls of the cavity for the temperature:

Boundary condition in the inlet opening of the flow of mixture air- H_2O	$T=T_{inlet}$
Boundary conditions in the outlet opening of the flow of mixture air- H_2O	$\frac{\partial T}{\partial n}=0$
Boundary condition of the interior surface of the conductive wall	$q_{cond-muro}=q_{conv-int}$
Boundary condition of any other surface of the cavity	$\frac{\partial T}{\partial n}=0$

where n is the normal vector to the direction of the flow

Boundary conditions in the walls of the cavity for the concentration of chemical species:

Boundary conditions for the chemical concentration	
Boundary condition in the inlet opening of the flow of mixture air- H_2O	$C=C_{inlet}$
Boundary conditions in the outlet opening of the flow of mixture air- H_2O	$\frac{\partial C}{\partial n}=0$
Boundary condition of the interior surface of the conductive wall	$C=C_{source}$
Boundary condition of any other surface of the cavity	$\frac{\partial C}{\partial n}=0$

where n is the normal vector to the direction of the flow

Boundary conditions in the walls, inlets and outlets of the cavity for the flow of air-H₂O mixture for turbulent variables:

Boundary conditions for the turbulent variables		
	(<i>k</i>)	(<i>ε</i>)
Boundary condition in the inlet opening of the flow of mixture air-H ₂ O	$k_{in}=1.5(0.04u_{in})^{2.0}$	$\epsilon_{in}=(k_{in})^{0.5}/(0.1H_i)$
Boundary conditions in the outlet opening of the flow of mixture air-H ₂ O	$\frac{\partial \epsilon}{\partial n}=0$	$\frac{\partial k}{\partial n}=0$
Boundary condition of any other surface of the cavity	Fixed values [Henkes, Van Der Vlugt and Hoogendoorn (1991)].	

Once the mathematical model of the ventilated cavity and the boundary conditions for the outlets and inlets, and the solid walls are established, the following considerations are taken into account to simplify the study model: steady state, two-dimensional flow, Newtonian and incompressible fluid, turbulent flow regime, constant thermo-physical properties, for the term of buoyancy forces the Boussinesq approximation is used, the effect of viscous dissipation is neglected, the mixture diffusion coefficient for low concentrations is considered, and finally the system of differential equations that model the flow are averaged over time.

Fig. 2 shows the physical model of the conductive wall, in which the horizontal surfaces are considered thermally insulated. On the right surface a constant and uniformly distributed heat flow is imposed, this heat flow is transported to the left surface by conduction, this left surface interacts with the fluid inside the cavity.

Considering that the conductive wall extends sufficiently in the third axis (z) to not affect the results in heat transfer, then the equation that governs the heat transfer in the solid wall is the two-dimensional heat conduction equation:

$$\frac{\partial}{\partial x_i} \left(\lambda_m \frac{\partial T_m}{\partial x_i} \right) = 0 \tag{10}$$

where λ_m , is the thermal conductivity and T_m is the temperature at the wall.

3.1 Boundary conditions of the conductive wall

Next, the boundary conditions of the conductive wall system, coupled to the ventilated cavity, are presented.

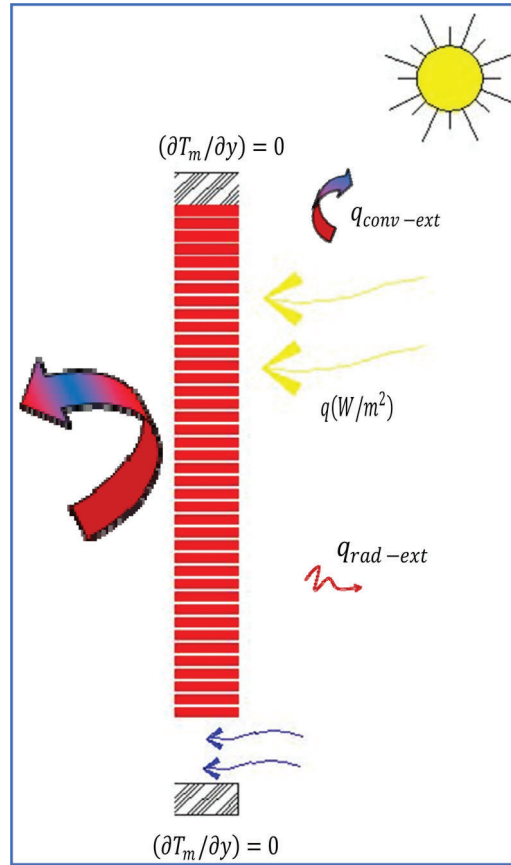


Figure 2: Physical model of the conductive wall

The inferior boundary of the conductive wall is considered as adiabatic

	In the direction of the horizontal component	At the selected height of the conductive wall
$\frac{\partial T_m}{\partial y} = 0$	$0 \leq x \leq H_m$	$y = H_i$

The superior boundary of the conductive wall is considered as adiabatic

$\frac{\partial T_m}{\partial y} = 0$	$0 \leq x \leq H_m$	$y = H_y$
---------------------------------------	---------------------	-----------

The right boundary of the opaque wall

$q_{total} = q_{cond-muro} + q_{rad-ext} + q_{conv-ext}$	(11)
$q_{total} = \lambda_m \frac{\partial T_m}{\partial x} + \sigma \varepsilon (T_m^4 - T_{ext}^4) + h(T_m - T_{ext})$	

The left boundary of the opaque wall

$q_{cond-muro} = q_{conv-int}$

The right boundary of the wall is subjected to a constant heat flux with losses by convection and radiation to the outdoor environment with outdoor temperature T_{ext} . The left boundary of the wall is interacting with the interior of the cavity, it is considered that the heat flow by conduction in the opaque wall is equal to the heat flow transmitted by convection through the air at a point very close to the wall, $q_{cond-muro}=q_{conv-int}$.

4 Calculation of the thermophysical properties of the air-H₂O mixture

To analyze the mixture of air-H₂O it is required to determine its thermo-physical properties; this calculation is done with the methodology presented by Reid et al. [Reid, Prausnitz and Poling (1987)] and Bird et al. [Bird, Stewart and Lightfoot (2006)]. The conditions under which the properties of the mixture were calculated for this study were at an average temperature of (24°C) and at the pressure of one atmosphere. To find the thermo-physical properties of the air-H₂O mixture first, we found the value of the property for each component of the mixture individually, once the value is found individually, the value is found as a chemical mixture. In the methodology, it is necessary to know the mass fraction of each component of the mixture. The calculation of the density was made with the equation of state for the ideal gases for each element. Subsequently, for the calculation of the viscosity of the air-H₂O mixture, the thermal conductivity of the air-H₂O mixture, and the mass diffusion of the air-H₂O mixture we used the Chapman-Enskog methodology presented in Reid et al. [Reid, Prausnitz and Poling (1987)]. In the case of the viscosity and the mass diffusion of the air-H₂O mixture, it was necessary to know the collision integral which was obtained from tables or could be calculated by a correlation. For the calculation of the specific heat of the air-H₂O mixture, it was carried out through a relationship as a function of temperature [Perri (1997)].

5 Numerical model of the heat and mass transfer of the air-H₂O mixture

This section we describe in a general way the methodology for the numerical solution of the mathematical model. The solution of the equations was obtained through the Finite Volume Method (FVM). The conservative equations are discretized and represented by a generalized equation (convection-diffusion). The SIMPLEC algorithm was used to couple the continuity equation and the momentum. The FVM consists of dividing the domain of the study into a finite number of control volumes, ordered consecutively without overlapping. In this method, the integral form of the conservation equations is used, which are used at each point (node) of the grid. These nodes are set intentionally in the center of each control volume (CV), for the calculation of the dependent variable. The numerical methodology is summarized in the following steps: (1) define and generate a numerical mesh, which represents the domain of the calculation in which we want to know the value of the dependent variables. (2) Integration and discretization of the governing equations of the phenomenon being studied, on all the control volumes of the domain of the solution. (3) Solution of the algebraic equations using an iterative algorithm.

The next flow diagram, Fig. 3, shows the iterative method used for solving the governing equations to obtain the variables of interest.

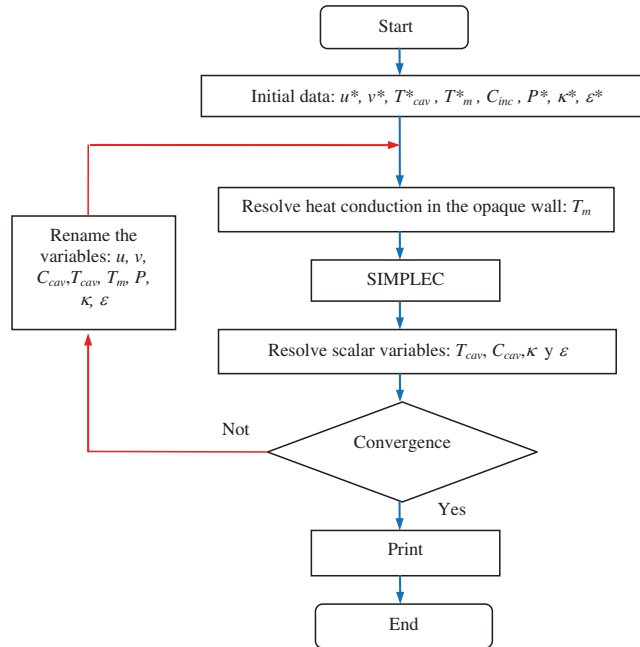


Figure 3: General algorithm of the convection-conduction-mass solution

To solve the problem of the numerically ventilated cavity an initial grid of 71×61 computational nodes was proposed, later the number of nodes was increased by 10 in 10 until having a grid of 121×111 computational nodes. The critical values of the variables were considered until obtaining a deviation of the computational error of 1.0% with a mesh of 111×110 computational nodes.

5.1 Validation of the numerical code for modeling the ventilated cavity

To validate the developed numerical code, the results provided by this code were compared with two solutions found in the literature. The first case was to validate the turbulence model presented by Henkes et al. [Henkes, Van Der Vlugt and Hoogendoorn (1991)] in which we compared the average Nu number ($Nu_{average}$), the Nu number in the center of the vertical wall of the cavity $Nu(y=H_y/2)$, the maximum Nu number (Nu_{max}), the vertical component of velocity at the center of the vertical wall $v_{max}/(g\beta\Delta TH_y)(g\beta\Delta TH_y)^{1/2}(y=H_y/2)$, and the horizontal component of velocity at the center of the vertical wall $u_{max}/(g\beta\Delta TH_y)(g\beta\Delta TH_y)^{1/2}(x=H_x/2)$. From the results, it were found percentage differences of (7.07%), (0.68%), (2.69%), (0.59%), and (8.87%), respectively. One can find the complete Table of comparison in Serrano-Arellano et al. [Serrano-Arellano and Gijón-Rivera (2014)].

The other comparison of results for the numerical code was found in the literature an experimental work for a ventilated cavity in turbulent flow regime proposed by Nielsen

[Nielsen (1990)], Fig. 4, that consists of a cavity with dimensions of $3 \times 9 \text{ m}^2$ with an inlet and flow outlet on the vertical walls. The comparison of results was with the horizontal velocity component for four different positions in the cavity, the velocity along the y-axis was also compared at the position of $X^*=1.0$ and $X^*=2.0$, the velocities along the x-axis in the positions $Y^*=0.972$ and $Y^*=0.028$, more details of the comparison of the results can be found in a previous work of the authors [Serrano-Arellano, Xamán and Álvarez (2013)]. From the comparison of results, the maximum difference was 16.14%, which represents an acceptable difference for the numerical code. Once the numerical code has been validated, the results of the present study are obtained.

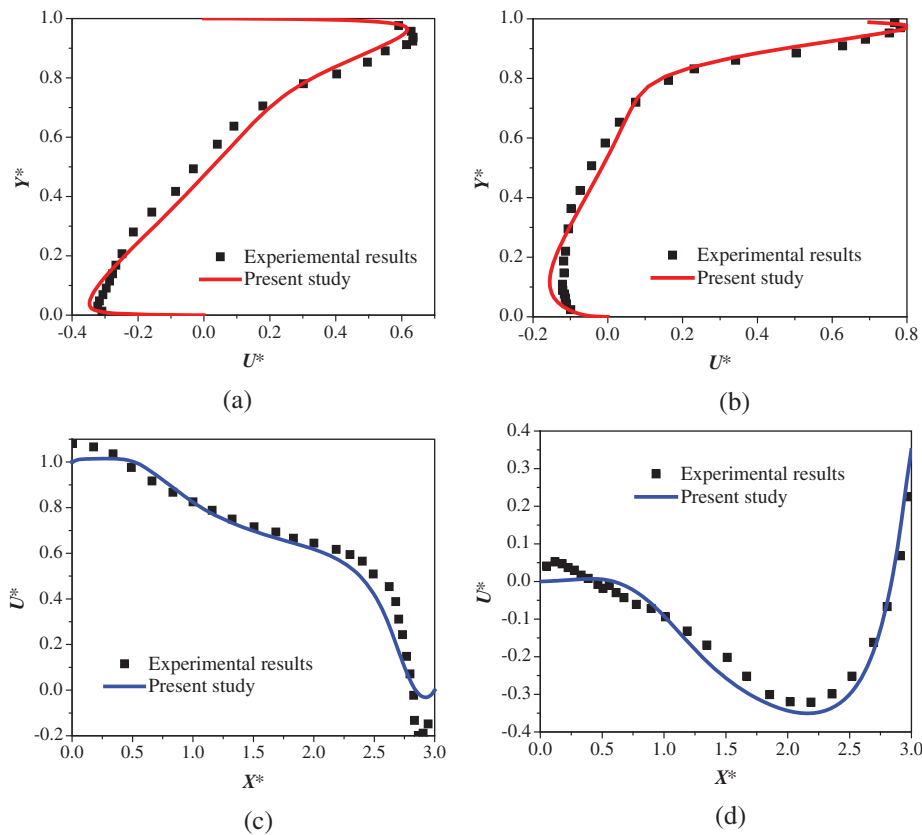


Figure 4: Comparison of the U^* velocity between Nielsen [Nielsen (1990)] and the present study in: (a) $X^*=1.0$, (b) $X^*=2.0$, (c) $Y^*=0.972$ and (d) $Y^*=0.028$

6 Number of Nusselt (Nu), Sherwood (Sh) and other characteristics parameters of the air- H_2O mixture

The number of (Nu) is the parameter commonly used to quantify the heat transfer in the ventilated cavity; this value is defined as the ratio of the magnitude of the heat transfer

by convection with respect to a reference heat flow [Oosthuizen and Naylor (1999)] define Nu as follows:

$$Nu = \frac{q_{conv-int}}{q_{ref}} \quad (12)$$

where (q_{ref}) is the reference heat flux or heat flux per conduction through the cavity that is defined by $q_{ref} = \lambda \frac{T_2 - T_1}{Hx}$, where (T_2) is the average temperature in the inner surface of the conductive wall of heat. (T_1) is the average temperature of the left vertical wall of the cavity. $q_{conv-int}$ is the heat transfer to the interior from the inner surface of the conductive wall, and is defined by:

$$q_{conv-int} = \lambda \left. \frac{\partial T(x,y)}{\partial x} \right|_{x=Hx} \quad (13)$$

The number of Sh indicates the total mass transfer within the cavity, this is defined as the ratio of magnitude of mass transfer by convection with respect to a reference mass flow and is expressed as follows:

$$Sh = \frac{C_{conv-int}}{C_{ref}} \quad (14)$$

where C_{ref} represents the reference mass flux which is given by $C_{ref} = D_{AB} \frac{C_2 - C_1}{Hx}$, where C_2 represents the average concentration at the surface of the pollutant source. C_1 represents the average concentration in the left vertical wall of the cavity. Finally, $C_{conv-int}$ represents the mass transfer of water vapor (H_2O) in the interior from the surface of the wall considered as a source of moisture concentration, this term is defined as:

$$C_{conv-int} = D_{AB} \left. \frac{\partial C(x,y)}{\partial x} \right|_{x=Hx} \quad (15)$$

The parameter overall ventilation effectiveness for temperature distribution represented by ($\bar{\epsilon}_t$) is important because in the study the maximum, minimum or average temperature values do not ensure that thermal comfort is achieved, thus it is necessary a parameter defining the homogeneity of the temperature in the distribution of the study space, Awbi [55] defines $\bar{\epsilon}_t$ in the following way:

$$\bar{\epsilon}_t = \frac{T_{outlet} - T_{inlet}}{T_{average} - T_{inlet}} \quad (16)$$

where T_{outlet} is the average temperature of the air- H_2O mixture at the opening of the outlet and $T_{average}$ is the average temperature of the air- H_2O mixture inside the cavity. Finally, T_{inlet} represents the average temperature of the air- H_2O mixture in the inlet opening of the ventilated cavity.

In the same way as defined ($\bar{\epsilon}_t$) is now defined ($\bar{\epsilon}_c$) that represents the overall ventilation effectiveness for *HR* distribution the maximum, minimum or average values of relative humidity (*RH*) of the air do not assure the hygrothermal conditions of the room, it is necessary to define a parameter that interprets the distribution of the *RH* inside the room. This parameter is defined according to Awbi [Awbi (2003)] as follows:

$$\bar{\epsilon}_c = \frac{C_{outlet} - C_{inlet}}{C_{average} - C_{inlet}} \quad (17)$$

where C_{outlet} is the average *RH* concentration of the air-H₂O mixture at the outlet opening and $C_{average}$ is the average *RH* concentration of the air-H₂O mixture within the cavity, and C_{inlet} represents the average *RH* concentration of the air-H₂O mixture at the inlet opening of the ventilated cavity.

7 Results and discussion

In this section the results found in the numerical study are shown, an analysis of the study variables was performed, the graphs of the velocity components, the temperature and the relative humidity percentages (*RH*) are presented. The values of *Nu* and *Sh* numbers are also shown to analyze the heat and mass transfer, respectively. The graphs of uniformity in the distribution of temperatures and the percentages of the relative humidity concentrations (*RH*'s) are also shown.

The study was conducted for the following records of weather conditions at 07:50, 10:00, 13:00, 14:00, 15:50, 17:50 and 21:00 h. The climatic record values were taken from the meteorological station located Cárdenas City of the State of Tabasco, Mexico on April 14, 2019. The state of Tabasco is one of the States with more humidity relative throughout the year in Mexico. From the weather record, variables such as solar radiation, outdoor temperature, concentration of the percentage of *RH* outside were taken into account. Tab. 1 shows a summary of the values of the parameters of the climatic conditions for the mentioned day.

The values represented in Tab. 1 were taken from the Lazaro Cardenas city campus national weather station and represent the weather data for different hours on a day in April. It is worth mentioning that the weather station is working by the standard NMX-AA-166/1-SCFI-2013 norm. The values of the variables for the conditions of the inflow velocities of the air-H₂O mixture flow into the room were estimated according to the ASHRAE standard [ASHRAE (2005)].

A flow of heat imposed on the outer surface of the concrete wall was considered due to the solar radiation incident on the right wall of the ventilated cavity, the construction material of the right wall was a lightweight concrete block of 12 cm wide as considered by Xamán et al. [Xamán, Tun, Álvarez et al. (2009)].

The thermo-physical properties of the air-H₂O mixture were calculated as the air-H₂O mass input conditions at the inlet opening of the ventilated cavity. A concentration of 20% for *RH*

Table 1: Outdoor weather conditions

Time (Hours)	Solar radiation (W/m^2)	Outdoor temperature ($^{\circ}C$)	Relative humidity (% of RH)
7:50	99	27.2	55
10:00	578	28.8	70
13:00	964	30.7	66
14:00	622	30.3	69
15:50	335	28.5	75
17:50	55	27.1	77
21:00	0	25.5	76

Note: National Weather Station (<https://smn.conagua.gob.mx/>)

was considered as water vapor in the air-H₂O mixture at the inlet of the cavity, considering that the percentage of the RH in the interior is higher considering that the percentage of the RH at outdoors is much greater than that considered in the inlet flow of the air-H₂O mixture.

The convective and radiative losses on the outer surface of the wall were considered with the convective coefficient h_{conv} of 6.8 W/m²K, this value was taken according to the recommendation of the standard ASHRAE [ASHRAE (2005)] corresponds to an air speed value 3 m/s. It was also considered that the values of wind speed on the study day ranged from 1.23 to 4.6 m/s, so this consideration is within the range of recorded values.

Different values of the Re number were considered, 500, 1000, 5000, and 10000 that represent the flow velocities of the air-H₂O mixture of 0.026, 0.053, 0.26 and 0.53 m/s, respectively. The flow temperature of the air-H₂O mixture at the inlet of the room was 20°C with an RH concentration of 0.00241 kg/m³, in its equivalence this value approximately represents 1490 ppm of H₂O vapor particles.

In Fig. 5 the flow patterns for the ventilated cavity for the Reynolds number values of 500, 1000, 5000 and 10000 were shown. The flow pattern for the value of $Re=500$ showed that forced convection at the entrance of the cavity was low enough not to transport the flow to the opposite wall, this generated a large area of flow stagnation in most of the cavity. For the value of $Re=1000$, forced convection gained strength and managed to bring the mass of the flow to the opposite area of the cavity. With the value of $Re=5000$, a flow recirculation was formed near the right wall where the flow inlet opening is located. With the value of $Re=10000$ a flow recirculation was formed in the lower area of the center of the cavity, the flow took enough intensity to evenly distribute the variables of temperature and concentration of pollutants.

The graphical results shown below were considered for $Re=500$. Fig. 6 shows the results of the velocity component along the x-axis; the values are for the seven weather records at different times during the day. Fig. 6 shows that the pattern of the velocity components has flows in favor and against it. In low values of Re , the effect of natural convection has

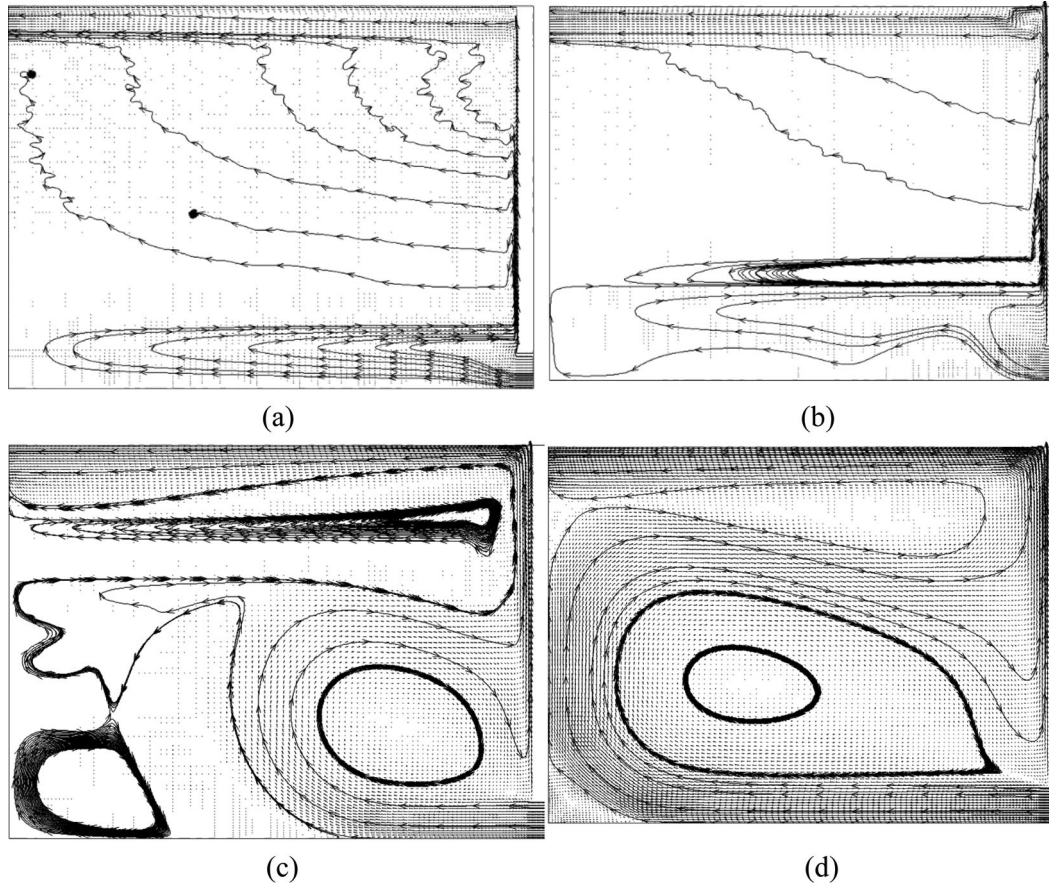


Figure 5: Flow patterns in the ventilated cavity for the different values of Re . (a) $Re=500$ (b) $Re=1000$ (c) $Re=5000$ and (d) $Re=10000$

a predominant presence, which causes recirculation of flow with advances and regression. It was observed that the components of the flow velocities of the air- H_2O mixture tend to have a recirculation as they approach the opposite wall where the outlet opening is located.

On the other hand, the highest values of the flow velocity components for the air- H_2O mixture occur next to the inlet opening and are presented at 13:00 h. These velocities are present because the wall receives the maximum solar radiation. However, movement in the mass of air is dominated by natural convection, which does not happen when forced convection begins to predominate.

[Fig. 7](#) shows that the behavior of the vertical velocity components in the flow pattern is similar near to the medium height of the cavity for any hour of the day. In other words, the flow pattern does not change at heights smaller than 1 m. Once the flow exceeds the height of one meter, the velocity components are dispersed with positive and negative

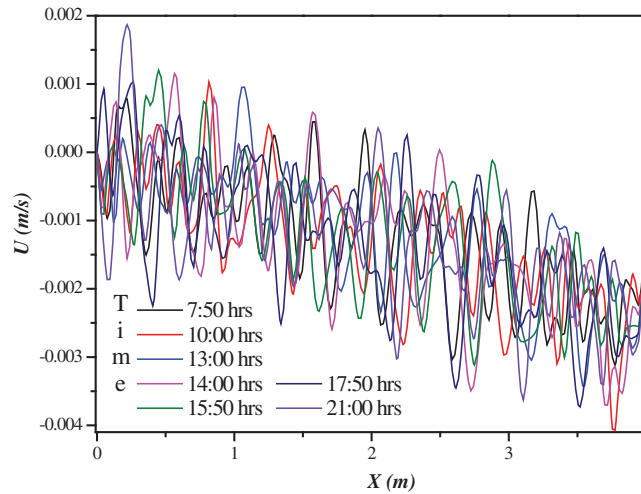


Figure 6: Behavior of the horizontal component of the velocity

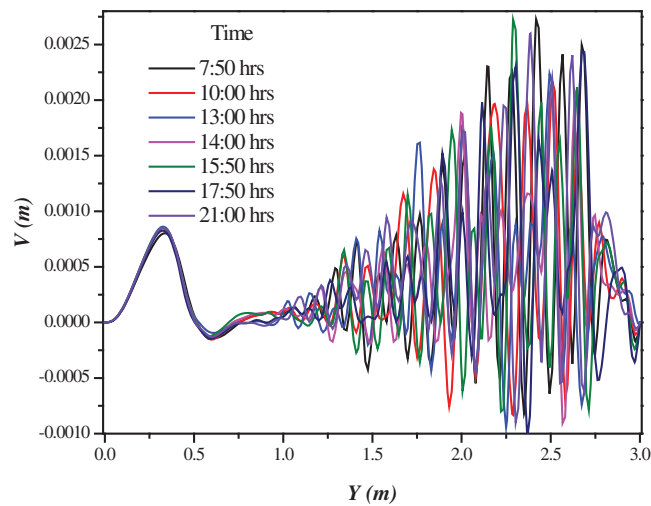


Figure 7: Behavior of the vertical component of velocity

values, which means that flow recirculation is present. Once the average height of the cavity is reached, the highest values of the vertical component of velocity are found at the height of 2.5 m, after this height, the flow becomes stabilized in the last 50 cm near the upper wall of the cavity.

Tab. 2 shows the values for the velocity components for all values of the number of Re at a central point in the cavity. The variation of the velocity components was observed for the different hours that were considered in the present study. The values shown in Tab. 2 showed changes in the flow direction, this was seen in the negative values. It was also

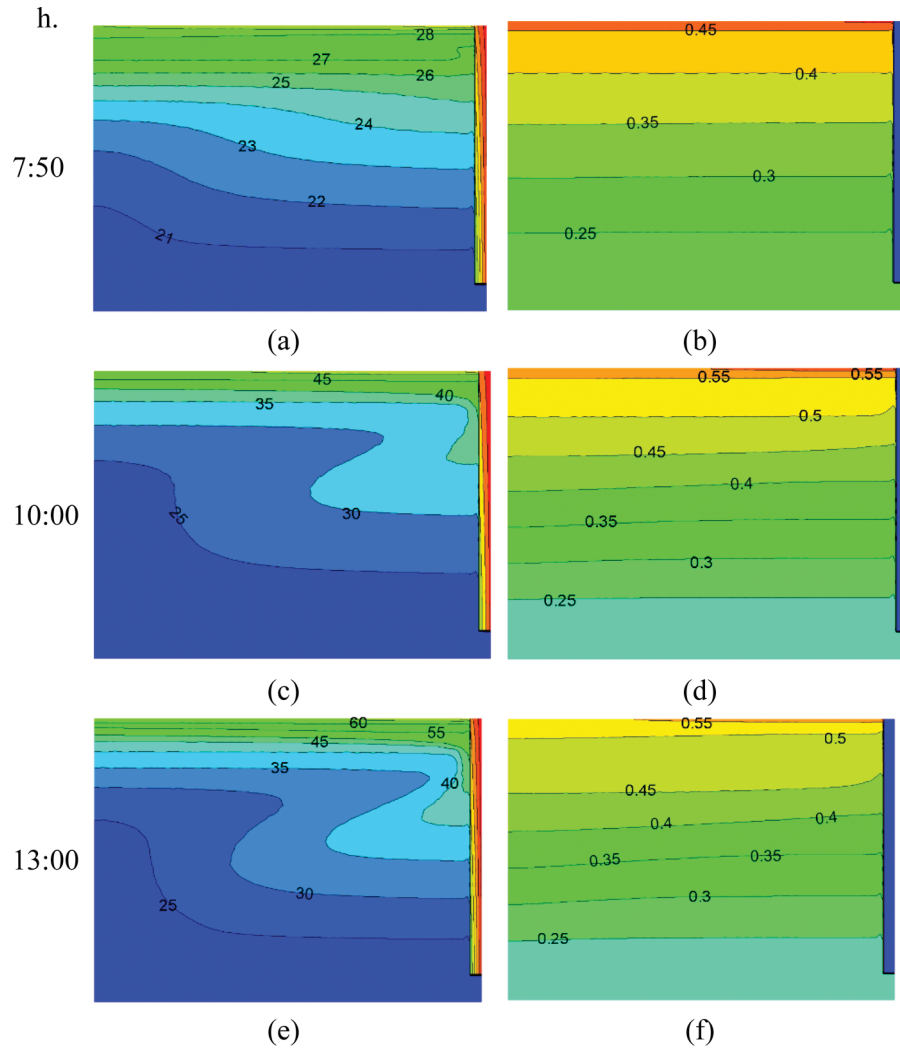
Table 2: Tabulation of the velocity components

Time	<i>Re</i> =500		<i>Re</i> =1000		<i>Re</i> =5000		<i>Re</i> =10000	
	u_x	v_y	u_x	v_y	u_x	v_y	u_x	v_y
7:50	-7.69E-04	-5.97E-05	-1.85E-04	-4.41E-05	6.19E-02	1.00E-01	1.45E-01	-7.03E-02
10:00	-1.27E-03	3.12E-04	-5.98E-04	2.04E-04	5.51E-02	8.73E-02	1.34E-01	-4.60E-02
13:00	-7.11E-04	1.95E-05	-4.12E-04	1.72E-04	5.46E-02	8.66E-02	1.33E-01	-4.54E-02
14:00	-1.04E-03	-1.34E-04	-2.47E-04	2.36E-04	5.51E-02	8.74E-02	1.34E-01	-4.60E-02
15:50	-7.07E-04	5.07E-05	-2.94E-04	1.86E-04	5.43E-02	8.65E-02	1.33E-01	-4.53E-02
17:50	-1.77E-03	3.76E-05	-5.68E-04	2.25E-04	5.55E-02	8.81E-02	1.34E-01	-4.68E-02
21:00	-5.02E-04	3.58E-04	-4.95E-04	6.78E-05	5.59E-02	8.90E-02	1.34E-01	-4.77E-02

observed that the high values of *Re*, that is, 5000 and 10000 the velocity components presented less change due to the dominant forced flow.

In Fig. 8 the behaviors of the temperature variables and relative humidity percentages with their numerical values for the ventilated cavity are appreciated. The values of the temperature and relative humidity variables were presented for the value of *Re*=500. It could be seen that by 7:50, 17:50 and 21:00 h the lowest temperature values were found inside the cavity. In the rest of the hours, high temperatures were reached inside the cavity in the upper area of the cavity. It was observed that the lowest temperatures occurred in the lower area of the cavity. Regarding relative humidity, the highest values were recorded at 9:00 p.m. with values of 65% relative humidity, that is, when there was no effect of solar radiation. It was observed that the lowest relative humidity values were obtained in the lower areas of the ventilated cavity. The rest of the hours of the day showed similar relative humidity values.

Fig. 9 shows the temperature components on the horizontal and vertical axes respectively, at different times of the day in the room. It can be observed that the highest temperatures are reached at 13:00 h, which is when the highest solar radiation was recorded with a value of 964 W/m², the second highest value of temperatures was with a solar radiation of 622 W/m² that was at 14:00 h, and so on, until reaching the lower values of temperature that was at 21:00 h, at night when the solar radiation was zero. At this time, a cooling of 20°C was reached in most of the room. It is important to note that there was a similar temperature in the room at 10:00 a.m. and at 2:00 p.m., because both hours had a solar radiation of 578 Wm⁻² and 622 W/m², respectively. In these cases, the outside temperature had a difference slightly greater than 1°C, and the difference of the percentages of *RH* was about 1%.

**Figure 8:** (continued)

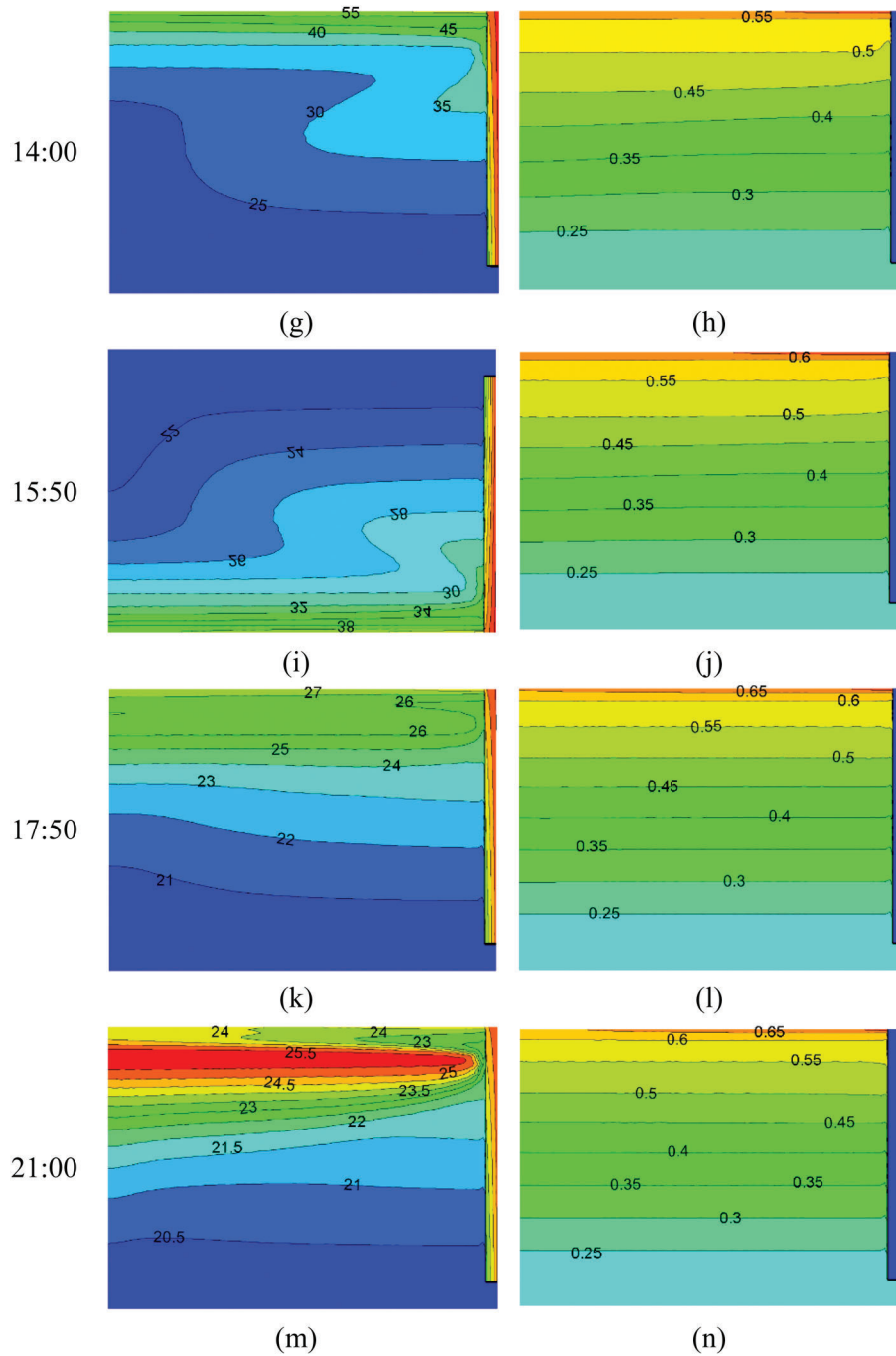


Figure 8: Behaviors of the temperature and relative humidity percentages ($\times 100\%$) for the value of $Re=500$

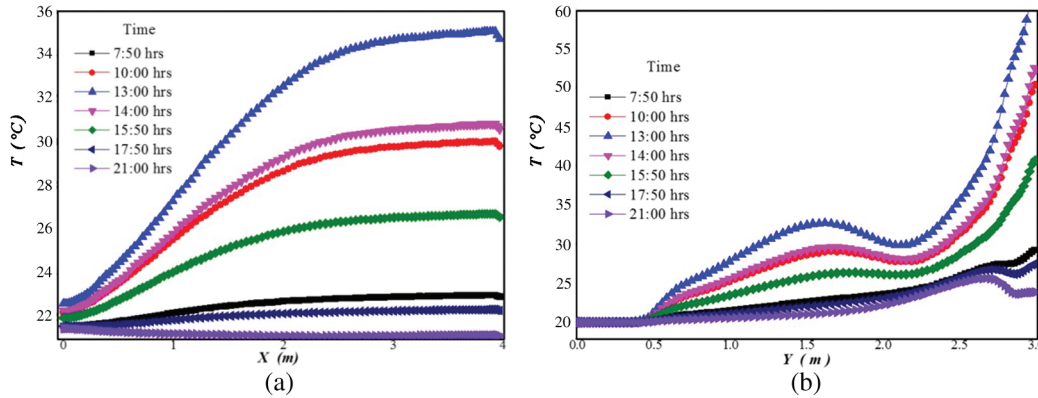


Figure 9: Temperatures $T(^{\circ}C)$ in the horizontal (a) and vertical (b) at the center of the ventilated cavity

Fig. 10 shows the behavior of the percentage of the RH in the room for seven different temperature records in the day. The effect of the percentage of the RH on the horizontal in the center of the ventilated cavity is observed in Fig. 10a. It is interesting to note that the values of percentage of RH in the horizontal of the cavity remain almost with constant values. Being the highest percentage value of the RH was 77% and occurred at 17:50 hrs. The lowest value occurred at 07:50 h, with a percentage of RH of 55% in the outdoor climate. However, in the horizontal axis at 17:50 h, the highest percentage of HR is reached with a value of 38.5%. On the vertical, higher values of percentage of RH than 60% are reached. This phenomenon occurs due to the convective movement of the flow of the air- H_2O mixture, due to the heating of the mass of the air- H_2O mixture tending to ascend to the high zones of the cavity. The heating of the air- H_2O mixture allows more

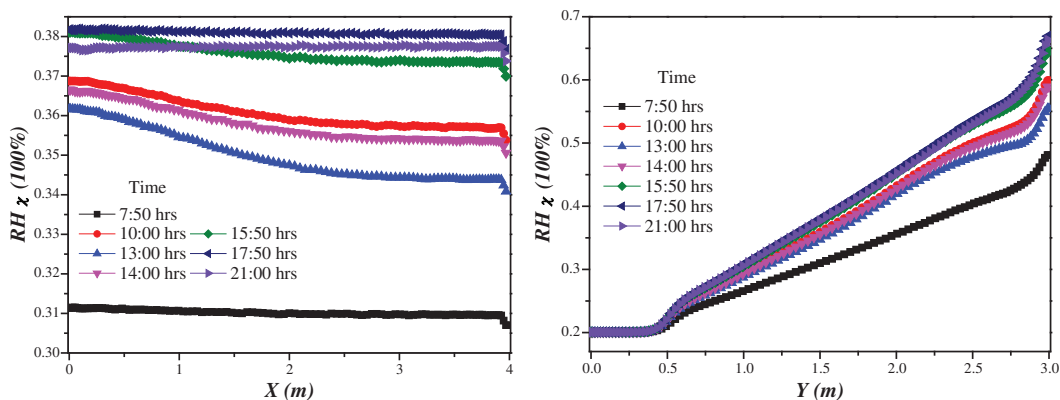


Figure 10: Percentages of RH in the horizontal (a) and vertical (b) of the center of the ventilated cavity

capacity of accumulation of H₂O vapor particles so that the concentration of water vapor in the form of *RH* is concentrated near the upper wall.

Fig. 11 shows the behavior of the heat transfer through *Nu* number values for different time records during the day. Fig. 11 shows that the maximum energy transfer occurs at 21:00 h. This is seen in the points near the inlet of the ventilated cavity. The values of the *Nu* number in the other time records tend to be equal. Although there is no heat flow due to the incident solar radiation on the outer surface of the wall, the highest value of the *Nu* number registered at 21:00 h, is due to the outdoor temperature conditions. It should be noted that the flow velocity value of the air-H₂O mixture at the inlet of the ventilated cavity was kept constant at different times of the day with a value of 0.026 m/s, this influenced the heat transfer in the convective effect.

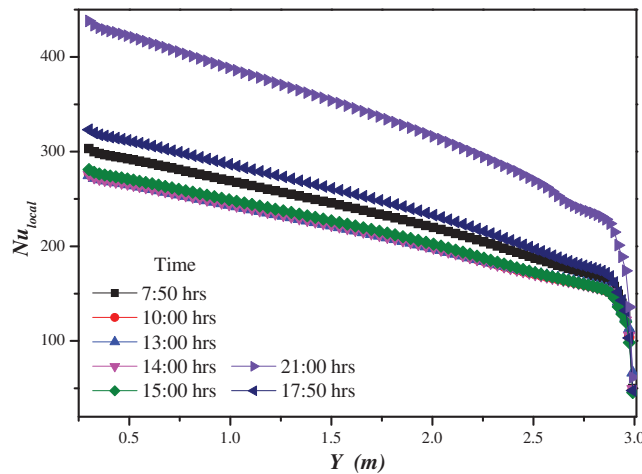


Figure 11: Values of the local *Nu* number on the vertical wall

Fig. 12 shows the behavior of the mass transfer through the number of *Sh*, which unlike the *Nu* number values, the mass transfer presents a similar behavior in all climatological records to throughout the hours of the day. This effect occurs because the *Sh* values depend mainly on the percentages of the *RH* concentration. The values of the *Sh* number are not affected by heat transfer because the Soret and Dufour effect was not taken into consideration [Mortimer and Eyring (1980); Hollinger and Lücke (1995)].

A comparison between the different *Re* numbers, Fig. 13, shows that the effect of the flow velocities of the air-H₂O mixture at the inlet opening of the ventilated cavity on the heat transfer. The values of *Nu* number are presented at 13:00 h when the maximum solar radiation is having an impact on the outer surface of the conductive wall. It was observed that the heat transfer through *Nu* number values for low values of the *Re* number tends to decrease as the height of the ventilated cavity is advanced. This effect was presented between the values of the *Re* number between 500 and 1000. A different effect occurs for

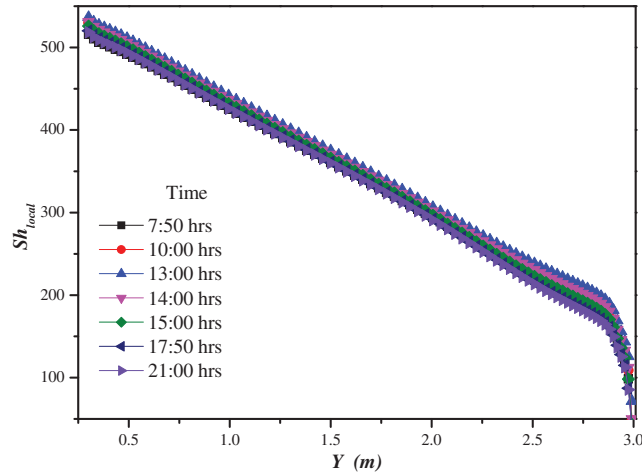


Figure 12: Values of the local Sh number on the vertical wall

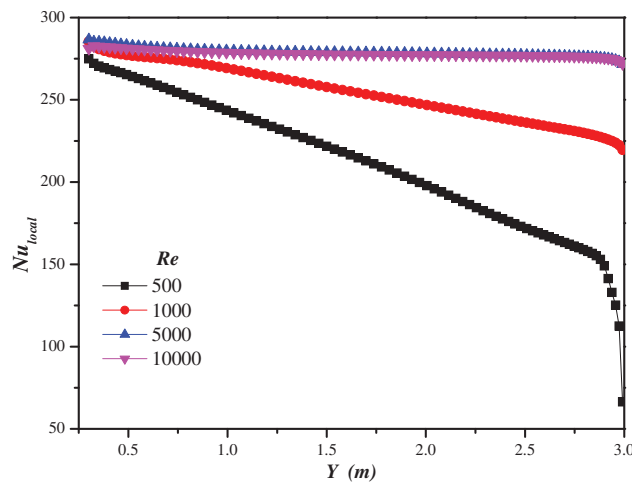


Figure 13: Values of the local Nu number on the vertical wall at 13:00 h

the Re number of 5000 and 10000, which means that the heat transfer is dominated by forced convection, therefore, it remains practically constant. That is, at high velocities of the mass flow rate of the air- H_2O mixture inside the ventilated cavity, they tend to homogenize the temperatures inside.

An interesting contribution of the present study is to compare the value of the Nu number for another record of the climate in an hour of the day when there is no incident radiative flow on the outer surface of the wall as it is at 21:00 h. It can be seen from Fig. 14 that the heat transfer with the highest values of local Nu to the lowest values of local Nu are presented for the value of Re of 500. This behavior is interesting because it was observed that the highest

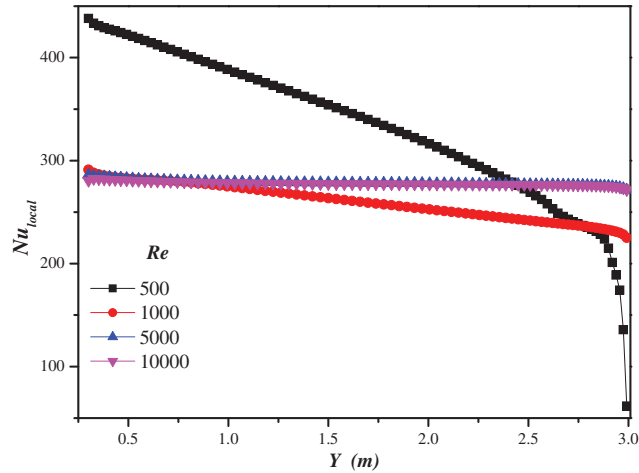


Figure 14: Values of the local Nu number on the vertical wall at 21:00 h

values of the heat transfer were for high numbers of Re . However, when there is no heat flow incident on the outer surface of the wall, i.e., a value of zero, which occurs at night, the heat transfer inside the ventilated cavity is due to the temperature conditions of the flow of the air- H_2O mixture at the inlet of the ventilated cavity.

The mass transfer is not affected at 13:00 h when there is a maximum incidence of solar radiation on the outer surface of the wall or with some other value of solar radiation. Fig. 15 shows a decrease in mass transfer for the lowest value of the Re number. The highest value of Sh number was around 550 occurred due to the predominant convective natural effect inside the ventilated cavity. The effect of the natural convective

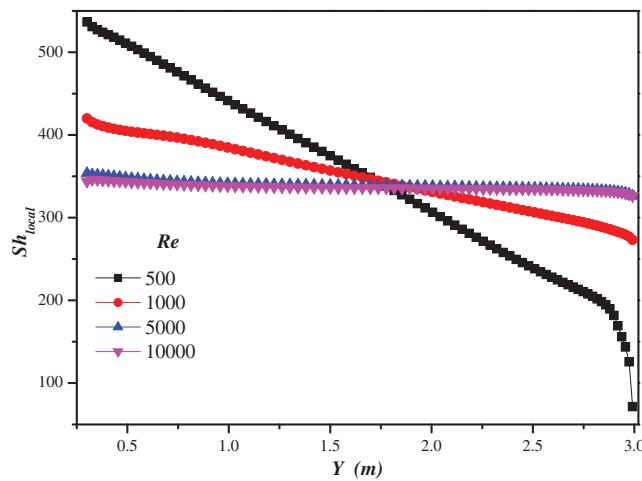


Figure 15: Values of the local Sh number on the vertical wall at 13:00 h

phenomenon can be seen by the behavior of the components of the flow velocities of the air-H₂O mixture in Figs. 6 and 7. In that figures can be seen the changes of direction of the flow velocity values of the air-H₂O mixture in the form of recirculation. At higher values of the Re number, that is, 5000 and 10000, the convective flow dominates the heat and mass transfer.

All the values of the Sh number were compared for all values of the number of Re in this study. It was observed that the Sh number for $Re=500$ is below the other values Sh from the average height of the ventilated cavity until the flow reaches the upper wall. It can be seen how the values of the Sh number in general decrease when the heat flow in the outer surface of the wall is reduced. This is because the heat and mass transfer depend on the temperature conditions of the flow of the air-H₂O mixture at the inlet of the ventilated cavity and the conditions of the concentration percentage of RH at the inlet of the ventilated cavity.

7.1 Effect of the overall ventilation effectiveness on temperature and concentration distributions

Fig. 16 shows the effect of temperature distribution and the percentages of RH inside the ventilated cavity. The lowest value of temperature distribution was presented for $Re=1000$ with maximum values of 30%. For $Re=500$ and $Re=1000$, the behavior between the distribution of temperatures and the percentages of RH are opposite; this effect is due to the influence of the natural convective effect. This behavior does not happen for the $Re=5000$ and $Re=10000$ when the forced convective effect is the dominant, the values of efficiency in the distribution of temperatures and percentages of RH are very similar reaching a maximum efficiency of 60%. It can be concluded that for higher values of efficiency, it is necessary to increase the flow velocities of the mixture at the inlet opening of the ventilated cavity. However, this is not the best option because it requires increasing the electrical power and it generates discomfort for users due to the high flow rates inside the ventilated cavity.

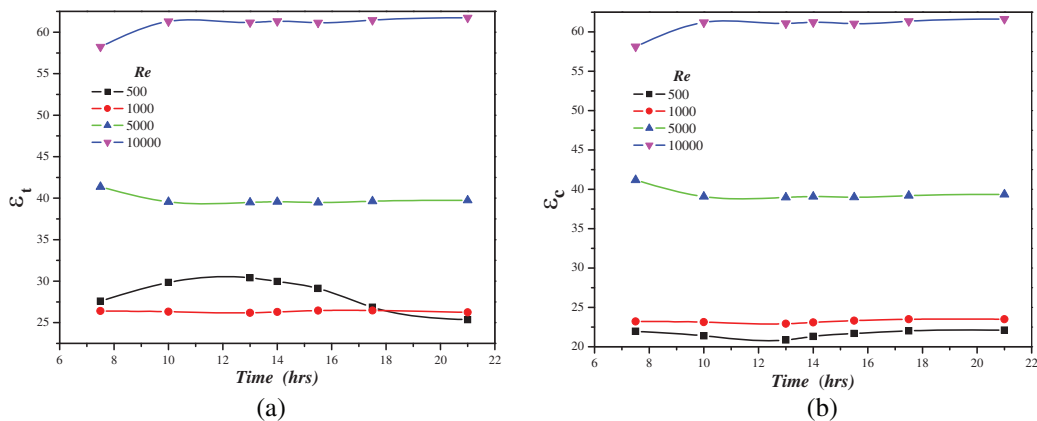


Figure 16: Values of overall ventilation effectiveness for temperature and concentration distributions ε_t and ε_c respectively

8 Conclusions

An analysis of the heat and mass transfer was carried out as concentration of the percentage of *RH* in a ventilated cavity where climatic parameters were varied in seven-time records throughout the day. The velocity of the flow in the inlet of the air-H₂O mixture was varied and it was found that for low values of the Reynolds number ($Re=500$) there is a movement predominantly by natural convection of the flow mass of the air-H₂O mixture. When the flow velocities at the inlet of the air-H₂O mixture increase, forced convection predominates in the cavity, this increases the costs by increasing the electric power to supply greater volume of the mass of the air-H₂O mixture flow. In most air conditioning (A/C) systems, which function as heat exchangers, they reduce the temperature of the air that is introduced to the A/C evaporator. However, an A/C reduces the percentage of *RH* in the air-H₂O mixture, this reduction causes that in the interior of buildings circulates air in low percentage of *RH* (around 20%). This type of conditions is not adequate, so it creates discomfort in users and generally results in colds or some other symptoms of illness related to cooling with dry air. On the other hand, the distribution of temperatures and *RH* percentages showed that a large amount of electric power is necessary to homogenize the interior, in this study only about 60% of distribution efficiency was achieved for both, the temperature and the percentage of *RH*. This effect occurred because the configuration is not optimal for homogeneously distributing the temperatures and the percentages of *RH*, it is recommended to continue with other studies to find the optimal configuration in which you can combine various factors such as natural convection, forced convection, values of temperature and percentages of concentration of *RH* in the inlet opening of the ventilated cavity and mainly the locations of the inlet and outlet flow openings.

Funding Statement: The author(s) received no specific funding for this study.

Conflicts of Interest: The authors declare that they have no conflicts of interest to report regarding the present study.

References

- Al-Kayiem, H. H.; Sreejaya, K. V.; Chikere, A. O.** (2018): Experimental and numerical analysis of the influence of inlet configuration on the performance of a roof top solar chimney. *Energy and Buildings*, vol. 159, pp. 89-98. DOI 10.1016/j.enbuild.2017.10.063.
- Arefmanesh, A.; Najafi, M.; Nikfar, M.** (2010): MLPG application of nanofluid flow mixed convection heat transfer in a wavy wall cavity. *Computer Modeling in Engineering & Sciences*, vol. 69, no. 2, pp. 91-117.
- ASHRAE** (2005): *Handbook of Fundamentals*. American Society of Heating, Refrigeration and Air Conditioning Engineers, New York.
- Awbi, H. B.** (2003): *Ventilation of Building*. 2nd Edition. Taylor & Francis Group. Spon Press, London.

Blazek, J. (2001): *Computational Fluid Dynamics: Principles and Applications*. Baden-Daettwil, Elsevier Science Ltd, Switzerland.

Bird, R. B.; Stewart, W. E.; Lightfoot, E. N. (2006): *Transport Phenomena*. 2nd Edition. John Wiley & Sons, Inc., New York, NY.

Das, D.; Basak, T. (2016): Role of distributed/discrete solar heaters during natural convection in the square and triangular cavities: CFD and heatline simulations. *Solar Energy*, vol. 135, pp. 130-153. DOI 10.1016/j.solener.2016.04.045.

Dou, H. S.; Jiang, G. (2016): Numerical simulation of flow instability and heat transfer of natural convection in a differentially heated cavity. *International Journal of Heat and Mass Transfer*, vol. 103, pp. 370-381. DOI 10.1016/j.ijheatmasstransfer.2016.07.039.

Harish, R. (2018): Effect of heat source aspect ratio on turbulent thermal stratification in a naturally ventilated enclosure. *Building and Environment*, vol. 143, pp. 473-486. DOI 10.1016/j.buildenv.2018.07.043.

Henkes, R. A. W. M.; Van Der Vlugt, F. F.; Hoogendoorn, C. J. (1991): Natural-convection flow in a square cavity calculated with low-Reynolds-number turbulence models. *International Journal of Heat and Mass Transfer*, vol. 34, no. 2, pp. 377-388. DOI 10.1016/0017-9310(91)90258-G.

Hollinger, S.; Lücke, M. (1995): Influence of the Dufour effect on convection in binary gas mixtures. *Physical Review E*, vol. 52, no. 1, pp. 642-657. DOI 10.1103/PhysRevE.52.642.

Huan, C.; Wang, F.; Wu, X.; Lin, Z.; Ma, Z. et al. (2018): Development of a nodal model for predicting the vertical temperature profile in a stratum-ventilated room. *Energy and Buildings*, vol. 159, pp. 99-108. DOI 10.1016/j.enbuild.2017.10.084.

Huang, J.; Yu, J.; Yang, H. (2018): Effects of key factors on the heat insulation performance of a hollow block ventilated wall. *Applied Energy*, vol. 232, pp. 409-423. DOI 10.1016/j.apenergy.2018.09.215.

Kefayati, G. H. R. (2017): Simulation of natural convection and entropy generation of non-Newtonian nanofluid in a porous cavity using Buongiorno's mathematical model. *International Journal of Heat and Mass Transfer*, vol. 112, pp. 709-744. DOI 10.1016/j.ijheatmasstransfer.2017.04.121.

Kefayati, G. H. R. (2019): Lattice Boltzmann method for natural convection of a Bingham fluid in a porous cavity. *Physica A: Statistical Mechanics and Its Applications*, vol. 521, pp. 146-172. DOI 10.1016/j.physa.2019.01.044.

Koufi, L.; Younsi, Z.; Cherif, Y.; Naji, H.; El Ganaoui, M. (2017): A numerical study of indoor air quality in a ventilated room using different strategies of ventilation. *Mechanics & Industry*, vol. 18, no. 2, pp. 221. DOI 10.1051/meca/2016043.

Kouroudis, I.; Saliakellis, P.; Yiantsios, S. G. (2017): Direct numerical simulation of natural convection in a square cavity with uniform heat fluxes at the vertical sides: flow structure and transition. *International Journal of Heat and Mass Transfer*, vol. 115, pp. 428-438. DOI 10.1016/j.ijheatmasstransfer.2017.08.058.

- Kumar, S.; Singh, M. K.; Mathur, A.; Mathur, J.; Mathur, S.** (2018): Evaluation of comfort preferences and insights into behavioural adaptation of students in naturally ventilated classrooms in a tropical country, India. *Building and Environment*, vol. 143, pp. 532-547. DOI 10.1016/j.buildenv.2018.07.035.
- Larsen, S.** (2006). *Natural Ventilation Driven by Wind and Temperature Difference (Ph.D. Thesis)*. Aalborg University, Denmark.
- Łukaszewicz, G.; Kalita, P.** (2016): *Navier-Stokes Equations: An Introduction with Applications*. Springer International Publishing, AG Switzerland.
- Macias-Melo, E. V.; Aguilar-Castro, K. M.; Xamán, J.; Hernández-Pérez, I.** (2018): Experimental study of convective heat transfer in a ventilated rectangular cavity. *Journal of Building Physics*, vol. 42, no. 3, pp. 388-415. DOI 10.1177/1744259118767197.
- Mehedi, T. H.; Tahzeeb, R. B.; Islam, A. S.** (2017): Numerical analysis of steady and transient natural convection in an enclosed cavity. *AIP Conference Proceedings*. vol. 1851, pp. 1-7. AIP Publishing LLC, Dhaka, Bangladesh.
- Miroshnichenko, I. V.; Sheremet, M. A.** (2018): Radiation effect on conjugate turbulent natural convection in a cavity with a discrete heater. *Applied Mathematics and Computation*, vol. 321, pp. 358-371. DOI 10.1016/j.amc.2017.11.010.
- Mortimer, R. G.; Eyring, H.** (1980): Elementary transition state theory of the Soret and Dufour effects. *Proceedings of the National Academy of Sciences of the United States of America*, vol. 77, no. 4, pp. 1728-1731. DOI 10.1073/pnas.77.4.1728.
- Nicolás, A.; Bermúdez, B.** (2011): 2D mixed convection viscous incompressible flows with velocity-vorticity variables. *Computer Modeling in Engineering & Sciences*, vol. 82, no. 3, pp. 163-178.
- Nielsen, P.** (1990): Specification of a two-dimensional test case, energy conservation in buildings and community system. Annex 20, Denmark, November.
- Oosthuizen, P. H.; Naylor, D.** (1999): *Introduction to Convective Heat Transfer Analysis*. McGraw-Hill Book Co., Singapore.
- Parmananda, M.; Dalal, A.; Natarajan, G.** (2018): The influence of partitions on predicting heat transfer due to the combined effects of convection and thermal radiation in cubical enclosures. *International Journal of Heat and Mass Transfer*, vol. 121, pp. 1179-1200. DOI 10.1016/j.ijheatmasstransfer.2018.01.031.
- Perri, R.** (1997): *Perry's Chemical Engineers Handbook*. Printed in the United States of America, Mc Graw Hill.
- Pretnel, H.** (2017): Interaction between water spray and smoke in a fire event in a confined and mechanically ventilated enclosure. *Fire Safety Journal*, vol. 91, pp. 336-346. DOI 10.1016/j.firesaf.2017.03.025.
- Raczkowski, A.; Suchorab, Z.; Polednik, B.; Zarzeka-Raczkowska, E.; Życzyńska, A.** (2018): Computational fluid dynamics simulation of thermal comfort in naturally ventilated room by the fresh air valve installed in an external wall. *AIP Conference Proceedings*, vol. 1988, no. 1, pp. 1-6. AIP Publishing LLC. Smolenice, Slovakia.

- Reid, R. C.; Prausnitz, J. M.; Poling, B. E.** (1987): *The Properties of Gases and Liquids*. 4th Edition. Mc Graw Hill Book Co., New York, NY.
- Serrano-Arellano, J.; Xamán, J.; Álvarez, G.** (2013): Optimum ventilation based on the ventilation effectiveness for temperature and CO₂ distribution in ventilated cavities. *International Journal of Heat and Mass Transfer*, vol. 62, pp. 9-21. DOI 10.1016/j.ijheatmasstransfer.2013.02.051.
- Serrano-Arellano, J.; Gijón-Rivera, M.** (2014): Conjugate heat and mass transfer by natural convection in a square cavity filled with a mixture of Air-CO₂. *International Journal of Heat and Mass Transfer*, vol. 70, pp. 103-113.
- Shi, Y. S.; Liu, D.; Wang, Y.; Zhao, F. Y.; Li, Y. X.** (2019): Forced flow structure and mixed convection in a ventilated porous enclosure with a local contaminant source. *International Journal of Heat and Mass Transfer*, vol. 131, pp. 973-983. DOI 10.1016/j.ijheatmasstransfer.2018.09.096.
- Singh, M. K.; Kumar, S.; Ooka, R.; Rijal, H. B.; Gupta, G. et al.** (2018): Status of thermal comfort in naturally ventilated classrooms during the summer season in the composite climate of India. *Building and Environment*, vol. 128, pp. 287-304. DOI 10.1016/j.buildenv.2017.11.031.
- Wang, Y.; Chen, Y.; Li, C.** (2019): Airflow modeling based on zonal method for natural ventilated double skin façade with Venetian blinds. *Energy and Buildings*, vol. 191, pp. 211-223. DOI 10.1016/j.enbuild.2019.03.025.
- Xamán, J.; Tun, J.; Álvarez, G.; Chavez, Y.; Noh, F.** (2009): Optimum ventilation based on the overall ventilation effectiveness for temperature distribution in ventilated cavities. *International Journal of Thermal Sciences*, vol. 48, no. 8, pp. 1574-1585. DOI 10.1016/j.ijthermalsci.2008.12.008.
- Xamán, J.; Gijón-Rivera, M.** (2015): *Dinámica de Fluidos Computacionales para Ingenieros*. 1st Edition, 47403, Palibrio, Bloomington, IN.
- Yu, J.; Yang, J.; Xiong, C.** (2015): Study of dynamic thermal performance of hollow block ventilated wall. *Renewable Energy*, vol. 84, pp. 145-151. DOI 10.1016/j.renene.2015.07.020.
- Yamamoto, T.; Ozaki, A.; Lee, M.; Kusumoto, H.** (2018): Fundamental study of coupling methods between energy simulation and CFD. *Energy and Buildings*, vol. 159, pp. 587-599. DOI 10.1016/j.enbuild.2017.11.059.
- Yao, T.; Lin, Z.** (2014): An experimental and numerical study on the effect of air terminal types on the performance of stratum ventilation. *Building and Environment*, vol. 82, pp. 431-441. DOI 10.1016/j.buildenv.2014.09.021.
- Zhang, S.; Cheng, Y.; Fang, Z.; Huan, C.; Lin, Z.** (2017): Optimization of room air temperature in stratum-ventilated rooms for both thermal comfort and energy saving. *Applied Energy*, vol. 204, pp. 420-431. DOI 10.1016/j.apenergy.2017.07.064.